Results in Materials xxx (xxxx) 100312

Contents lists available at ScienceDirect

Results in Materials

journal homepage: www.elsevier.com

Journal Cover Image

# Determination of transverse isotropic elastic constants of nacre and constituent tablets based on genetic-algorithm-assisted resonant ultrasound spectroscopy

Go Yamamoto [a, b, *], Kazuma Matsui [a], Shuma Yuki [a], Ji Won Suk [b, c, d]

[a] Department of Aerospace Engineering, Tohoku University, 6-6-01 Aramaki-Aza-Aoba, Aoba-ku, Sendai 980-8579, Japan
[b] School of Mechanical Engineering, Sungkyunkwan University, Suwon, 16419, Republic of Korea
[c] SKKU Advanced Institute of Nanotechnology (SAINT), Sungkyunkwan University, Suwon 16419, Republic of Korea
[d] Department of Smart Fab. Technology, Sungkyunkwan University, Suwon 16419, Republic of Korea



ARTICLE INFO

*Keywords:*
Mechanical properties
Finite element analysis (FEA)
Non-destructive testing

ABSTRACT

Novel classes of tough composites inspired by natural biological materials like nacre, which possesses a multi-scale structure with a lamellar microarchitecture, have attracted significant attention for use in structural and energy-related applications. The current theoretical understanding of the toughening and deformation mechanisms of nacre, which could serve as guidelines for composite development, is based on limited material parameters. Here, we report an experimental and numerical study on the transverse isotropic elastic constants of nacre and its constituent inorganic tablets based on genetic-algorithm-assisted resonant ultrasound spectroscopy. The results show that, among the five elastic constants measured, the out-of-plane and in-plane Young's moduli of nacre sampled from *Pinctada martensii* were 72.3 ± 1.7 and 74.8 ± 2.0 GPa, respectively. The remaining out-of-plane and in-plane Poisson's ratios and out-of-plane shear modulus were 0.23 ± 0.01, 0.24 ± 0.04, and 21.3 ± 0.9 GPa, respectively. Similar trends were observed for the constituent tablets, however, the Young's moduli were slightly higher at 72.7 and 75.0 GPa, respectively. These results concerning the transverse isotropic elastic properties of nacre and its constituent tablets aid in realizing the bio-duplication of novel nacreous composite materials.

## 1. Introduction

Some biological species in nature exhibit unique mechanical characteristics by integrating inorganic ceramics with organic polymers in a distinctive manner. Among them is nacre, which consists of ~95 vol% inorganic polygonal tablets and only a minor percentage of organic interlayer polymers arranged in a brick-and-mortar-like microstructure, resulting in outstanding mechanical characteristics, including a combination of toughness and impact resistance. These properties have motivated researchers to understand its toughening mechanisms [1–12] and reproduce biomimetic composite materials based on its microstructural features [14–17].

Numerous studies have been devoted for revealing the possible mechanisms underlying the unique mechanical behavior of nacre materials from various points of view, including nanosize asperities on the tablets [3,6], their hierarchical structures [2,18–21], and the effect of the interlocked tablets and interlayers on the mechanical properties [22,23]. Wang et al. [3] investigated the inelastic deformation mechanism of nacre under external loads, with a focus on the nanosize mineral asperities present on the surface of the aragonite tablets. They revealed that the stress at which the inelastic deformation proceeds is governed by the asperities, and their interposing arrangements between the tablets dictate the sliding resistance subject to an initial strain hardening that facilitates the ductility. Young's moduli in the in-plane directions (edge-on and face-on directions) determined from the initial linear elastic region were essentially the same, averaging 73 GPa. Gao et al. [21] discussed the fracture strength of inorganic tablets with a thumbnail-like crack based on a Griffith criterion assuming an isotropic body with a Young's modulus of 100 GPa. They also proposed an optimum tablet aspect ratio by a virtual internal bond method, which implements an atomic cohesive force law into the constitutive material model, to describe the fracture mechanism of nanosize materials. Recently, Cui et al. [23] developed a closed-form analytical solution for bio-inspired nacreous composite materials with interlocked brick-and-mortar structures considering the influence of the tension zones in an interlayer material. Assuming isotropic tablets with a Young's modulus

* Corresponding author. Department of Aerospace Engineering, Tohoku University, 6-6-01 Aramaki-Aza-Aoba, Aoba-ku, Sendai 980-8579, Japan.
*E-mail address:* gyamamoto@tohoku.ac.jp (G. Yamamoto).

https://doi.org/10.1016/j.rinma.2022.100312
Received 19 May 2022; Received in revised form 3 August 2022; Accepted 22 August 2022
2590-048/© 20XX

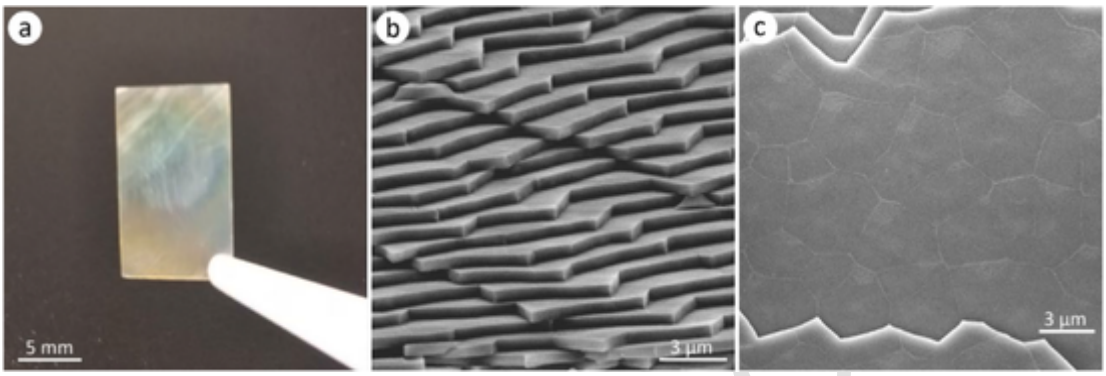


**Fig. 1.** (**a**) Photograph of the nacre sample subjected to vibration testing. (**b**,**c**) Electron microscope images of nacre fracture surfaces showing the lamellar structure consisting of polygonal tablets and thin interlayers.

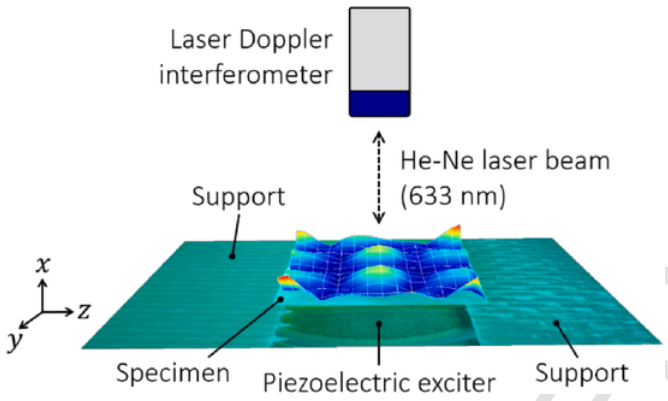


**Fig. 2.** Experimental setup for resonance spectrum and harmonic vibration pattern measurements.

of 100 GPa, they found that the mechanical characteristics of nacreous composites can be optimized by tailoring the length of the tablet and the interlocking angle.

Because of the limited accuracy of nacre material parameters, a wide range of moduli have been applied for modeling purposes. For the tablets, isotropic elasticity with Young's moduli in a wide range from 50 GPa to 100 GPa have been employed [3,24–30], and moduli for interlayer materials ranging from 2.84 to 49 GPa have been used [25,26,31–34]. As nacre and its constituent tablets could possess transversely isotropic characteristics owing to their geometric features, the quality of calculated predictions of their properties will inevitably suffer from a lack of accurate elastic modulus information. As mentioned above, previous research on nacre has exclusively focused on its toughening and deformation mechanisms and on developing tough composites. In contrast, this work focused on measuring the transverse isotropic elastic constants of nacre and its constituent polygonal tablets based on a genetic-algorithm-assisted resonant ultrasound spectroscopy technique.

## 2. Methods

**Sample preparation and resonance frequency measurements.** A nacre material sampled from *Pinctada martensii* (Uwajima, Japan) was mechanically polished into a sample of dimensions 9.033 mm (width) × 11.312 mm (length) × 0.185 mm (thickness), such that the basal plane was parallel to the in-plane direction of the polygonal tablets. Fig. 1a shows the nacre sample that was subjected to vibration testing. Electron microscopy observations revealed that the tablets were arranged in a lamellar structure with some overlap (Fig. 1b) and were surrounded by a thin interlayer material (Fig. 1c) such that the cross section resembled a brick wall. Measurements of more than 200 tablets showed that the out-of-plane thickness and basal surface area were approximately 370 nm and 12 μm$^2$, respectively; these values are reasonably consistent with the literature [26,35]. The bulk density of the sample, calculated by dividing the mass by the volume, was 2.386 Mg/m$^3$; this value was considered for vibration analysis using the finite element (FE) method.

Fig. 2 schematically shows the experimental setup for measuring the resonance spectrum and harmonic vibration patterns of the nacre sample. A sinusoidal continuous wave signal to oscillate the nacre sample was indirectly applied through air by simply placing the sample on a custom-designed support such that it did not experience the out-of-plane displacement distribution of the piezoelectric exciter. This treatment allowed the sample to vibrate with no external force causing the motion. The resonance spectrum and vibration patterns were measured using a laser Doppler interferometer (PSV-500 Scanning Vibrometer, Polytec) [36]. Measurements in the frequency range from 50 to 250 kHz were carried out at room temperature (approximately 25 °C) under ambient conditions (approximately 45% relative humidity) using He–Ne laser with an excitation wavelength of 633 nm. As different material behaviors have been reported between dry and wet nacres [24], only dry nacre was considered in this study. Therefore, nacre sample subjected to vibration testing was stored at ambient temperature and humidity, following the manner of Jackson et al. [24].

**Determination of equivalent elastic constants of nacre.** The derivation of elastic constant tensors by resonant ultrasound spectroscopy (RUS) involves indirect iterative procedures. Using the sample dimensions, density, and resonance frequencies, the elastic constant tensor of solid materials can be theoretically calculated [37–41]. In this study, equivalent elastic constants were efficiently determined considering nacre as a homogeneous body by employing a genetic algorithm (GA) [42–44] to ensure that the resonance frequencies and corresponding harmonic vibration patterns acquired from FE analysis were equivalent to those obtained experimentally. The optimization procedures for the elastic constants can be found as Supplementary Fig. S1(a) online. Five elastic constants ($E^{n}_{xx}$, $E^{n}_{yy}$, $\upsilon^{n}_{xy}$, $\upsilon^{n}_{yz}$, and $G^{n}_{xy}$) were determined assuming the nacre possesses a transverse isotropic elastic body with five independent elastic constants $C_{ij}$:

$$[C_{ij}] = \begin{bmatrix} C_{11} & C_{12} & C_{12} & 0 & 0 & 0 \\ C_{12} & C_{22} & C_{23} & 0 & 0 & 0 \\ C_{12} & C_{23} & C_{22} & 0 & 0 & 0 \\ 0 & 0 & 0 & C_{44} & 0 & 0 \\ 0 & 0 & 0 & 0 & C_{55} & 0 \\ 0 & 0 & 0 & 0 & 0 & C_{55} \end{bmatrix} \quad (1)$$

where $C_{44} = (C_{22} - C_{23})/2$. A three-dimensional FE mesh with approximately 1.6 × 10$^5$ eight-node full-integration hexahedral elements was implemented for the eigenvalue analysis under free boundary con-

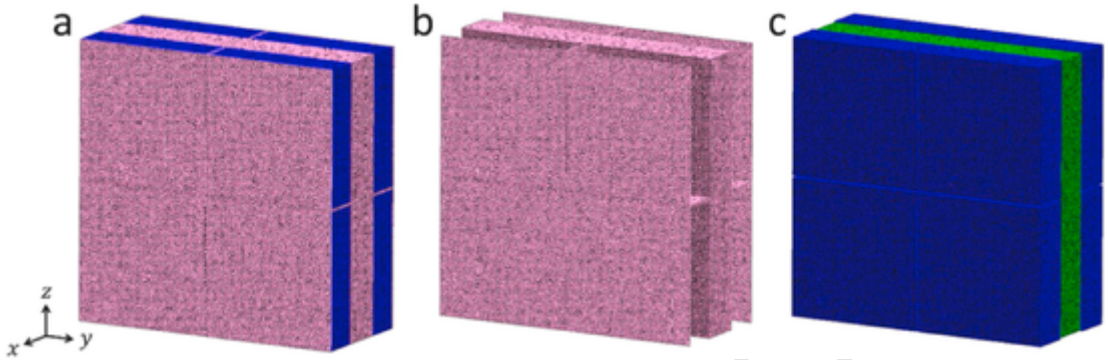


**Fig. 3.** (**a**) FE model for microscopic PUC analysis. (**b**) Thin interlayer domain and (**c**) tablet domain. The green and blue domains in (**c**) indicate one full tablet and eight cut-in-quarters tablets, respectively. In the composite model in figure (**a**), the green full tablet domain shown in image (**c**) is completely covered with the interlayer domain. (For interpretation of the references to colour in this figure legend, the reader is referred to the Web version of this article.)

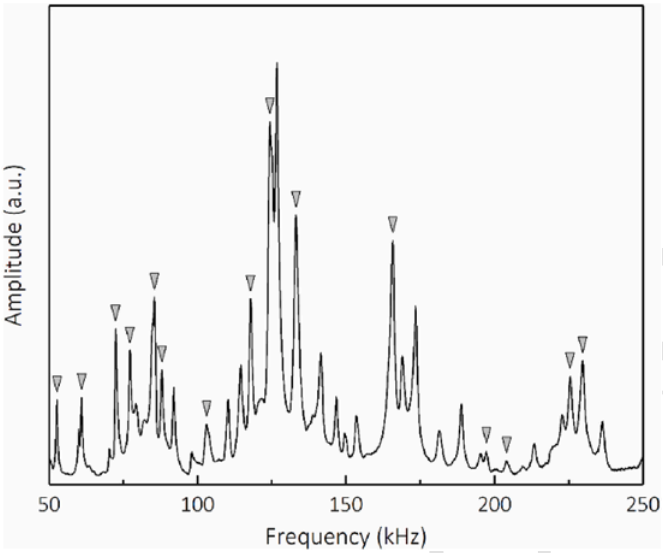


**Fig. 4.** Resonance spectrum of the nacre sample. The arrows indicate the 15 resonance peaks used in the $F_{\mathrm{RUS}}$ calculations.

ditions. Assuming that an initial estimate of material parameters is given, it is possible to assemble the stiffness $\boldsymbol{K}$ and mass $\boldsymbol{M}$ matrices and solve the generalized eigenvalue problem described below.

$$\boldsymbol{K}v_i = \lambda_i \boldsymbol{M}v_i \tag{2}$$

where $v_i$ is the eigenvectors and $\lambda_i = (2\pi f_i)^2$. Consequently, the resonance frequencies can be numerically determined by solving the eigenvalue problem using Lanczos eigensolver implemented in ABAQUS/Standard [45,46]. In the GA optimization, the elitist selection scheme was implemented to determine the next generation by excluding the best-fitting individuals of each generation, and the roulette selection scheme, which changes the selection probability according to the fitness, was adopted to determine the parent individuals to generate the next generation. The population size, number of generations, generation gap, probability of crossover, and probability of mutation as GA parameters were set at 100, 100, 0.9, 0.6, and 0.05, respectively. Details on the role of the GA's parameters can be found can be found elsewhere [47]. To evaluate the fitness of the resonance frequencies determined by the experiment and FE analysis, a fitness function $F_{\mathrm{RUS}}$ was defined and determined using equation (3):

$$F_{\mathrm{RUS}} = \sqrt{\frac{1}{N}\sum_{i=1}^{N}\left(\bar{f}_i - f_i\right)^2} \tag{3}$$

where $\bar{f}_i$ and $f_i$ are the $i$-th resonance frequencies determined by the experiment and FE analysis, respectively. Theoretically, $F_{\mathrm{RUS}}$ decreases to zero as the elastic constants input to the FE analysis approach their true values. However, the resonance frequencies $\bar{f}_i$ may not correspond fully to defined by the material constants because they are scattered by experimental errors. The search range of the five variables was determined to sufficiently encompass the previously reported elastic constants [3,23–29], which can be found as Supplementary Table S1 online. Three GA optimizations were performed under different initial conditions to obtain different elastic constants for the first generation. The standard deviation of the optimization results, in addition to the averaged values, are reported in subsequent sections. Please note that the inversion code was verified by two approaches, a benchmark problem and a test sample with known elastic constants, and found that it has a high search capability under the conditions used in this study (details can be found in the Supplementary Information).

**Determination of tablet elastic constants.** A three-dimensional periodic unit cell (PUC) mesh of approximately 2.1 × $10^6$ ten-node second-order tetrahedral elements was modeled based on SEM observations to determine the elastic constants of the polygonal tablets, assuming a known Young's modulus and volume fraction of the thin interlayer material. For the microscopic PUC analysis, a static-explicit FE code employing the direct sparse solver PARDISO [48], a direct method solver for simultaneous linear equations with sparse matrices, was developed and implemented to speed up the FE calculation. Fig. 3 depicts the FE composite model (Fig. 3a), interlayer domain (Fig. 3b), and polygonal tablet domain (Fig. 3c) used for microscopic PUC analysis. In this study, we assumed the geometrical configuration of the polygonal tablets to have a cuboid shape; hence, accurate modeling of the three-dimensional polygonal structure would be difficult. The tablet domain consisted of one full tablet and eight cut-in-quarters tablets (Fig. 3c), each separated by an interlayer domain (Fig. 3b). The ratios of the interlayer to tablet thickness in the out-of-plane ($x$-axis) and in-plane ($y$- and $z$-axes) directions are modeled to be 1:20 and 1:140, respectively. As the average thickness of the tablets determined by SEM was approximately 370 nm, the thickness of the interlayer material in the composite model corresponds to approximately 18.5 nm. The volume fraction of tablets was 95%. The tablets were modeled as transverse isotropic elastic bodies with five independent elastic constants, $C_{ij}$, as given in equation (1), while the interlayer material was assumed to be an isotropic elastic body. The tablets and interlayers were assumed to be perfectly bonded, in order to focus exclusively on the elastic constants.

The five individual elastic constants of the tablets were determined by employing the above-mentioned GA optimization procedures for obtaining elastic constants from the composite model equivalent to those determined by RUS. The elastic constants of the tablets were determined by applying three tensile deformations and three shear deforma-

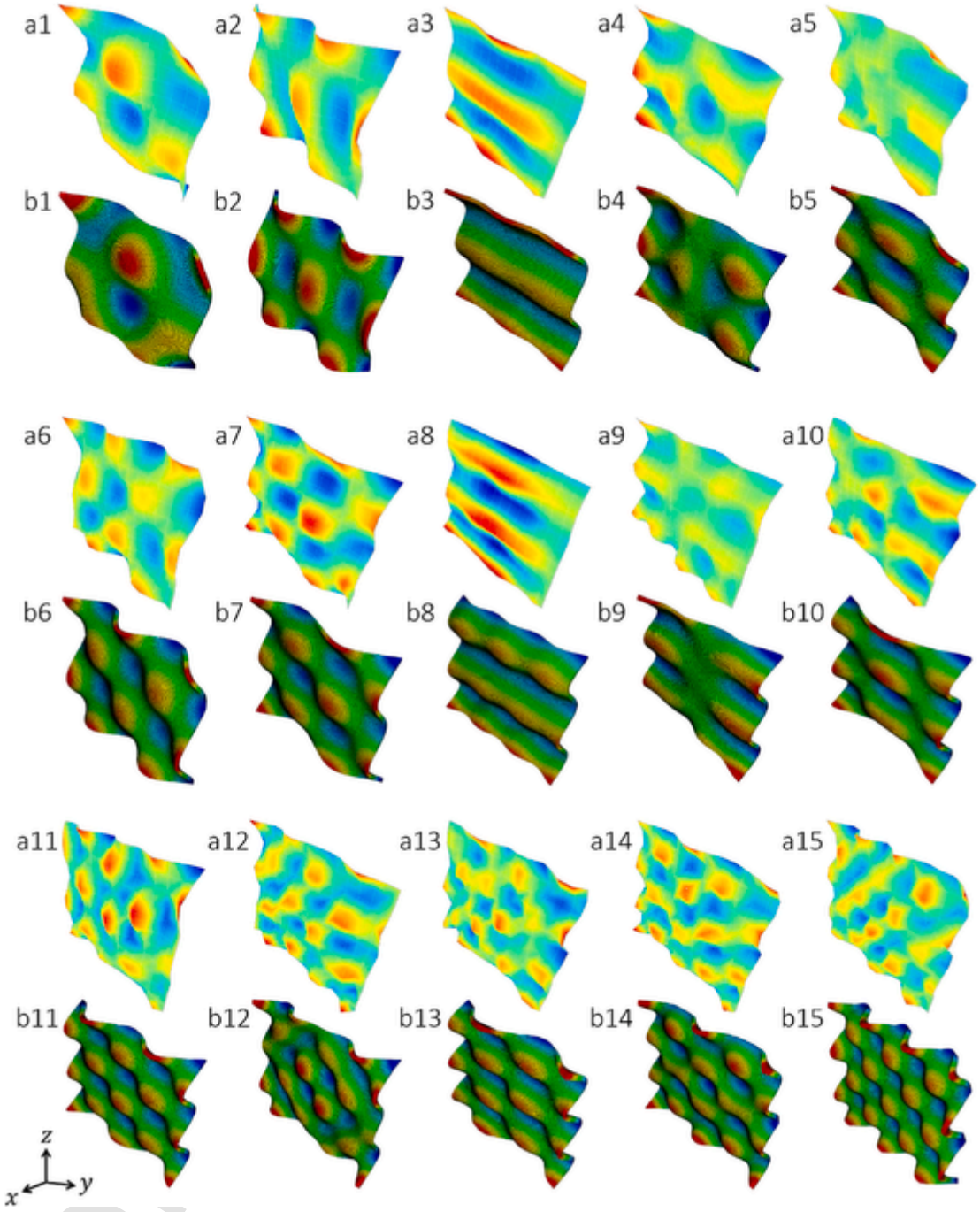


**Fig. 5.** Vibration patterns determined experimentally (**a1**–**a15**) and by preliminary FE analysis (**b1**–**b15**).

tions in each principal direction of the composite model (details can be found in the Supplementary Information). The Young's modulus and Poisson's ratio of the interlayer material were set to 11.3 GPa and 0.3, respectively, as determined by Xu et al. with the aid of a combination of three-point bending using atomic force microscopy and inverse FE analysis [34]. Based on the report by Xu et al. [34], the interlayer material exhibited a bilinear trend of elastic-inelastic deformation during loading, and the above-mentioned Young's modulus was determined from the initial elastic range. Possible mechanisms about the deformation behavior of the interlayer material can be found elsewhere [34]. The following equation was implemented to calculate the fitness $F_{\mathrm{PUC}}$ between the five elastic constants determined by PUC analysis and RUS.

$$F_{\mathrm{PUC}} = \sqrt{\frac{1}{5}\sum_{i=1}^{5}\left\{\log\left(D_i+1\right)-\log\left(\bar{D}_i+1\right)\right\}^2} \tag{4}$$

where $D_i$ and $\bar{D}_i$ are the equivalent elastic constants of nacre obtained from the PUC analysis and RUS, respectively; and $E^{\mathrm{n}}_{xx}$, $E^{\mathrm{n}}_{yy}$, $\upsilon^{\mathrm{n}}_{xy}$, $\upsilon^{\mathrm{n}}_{yz}$, and $G^{\mathrm{n}}_{xy}$ are parameters for the $F_{\mathrm{PUC}}$ calculation. In the PUC analysis, wherein five elastic constants are used to calculate the fitness, the root mean square logarithmic error (RMSLE) shown in equation (4) was used as the fitness function. The RMSLE is a metric that is used when the number of digits in the prediction differs significantly. The search range and resolution of the tablet elastic constants were identical to those of nacre. Optimization procedures for the tablet elastic constants

**Table 1**
Experimentally measured and numerically calculated resonance frequencies and the percentage errors between $\bar{f}_i$ and $f_i$. Results obtained from three GA optimization calculations are shown on columns 3 through 5. The percentage error for each calculation is indicated in parentheses.

| $i$ | Experiment, $\bar{f}_i$, kHz | FE calculation, $f_i$, kHz | | |
|---|---|---|---|---|
| | | 1st | 2nd | 3rd |
| 1 | 52.66 | 51.96 (1.35) | 51.77 (1.71) | 52.18 (0.92) |
| 2 | 60.00 | 62.49 (3.98) | 62.26 (3.63) | 62.35 (3.77) |
| 3 | 72.50 | 73.41 (1.24) | 72.95 (0.62) | 73.06 (0.77) |
| 4 | 77.19 | 76.90 (0.37) | 76.63 (0.73) | 77.43 (0.31) |
| 5 | 82.19 | 85.66 (4.05) | 85.45 (3.82) | 85.32 (3.67) |
| 6 | 87.97 | 88.76 (0.89) | 88.75 (0.88) | 88.30 (0.37) |
| 7 | 102.97 | 101.55 (1.40) | 101.79 (1.16) | 101.53 (1.41) |
| 8 | 117.81 | 117.09 (0.61) | 116.70 (0.95) | 116.57 (1.06) |
| 9 | 124.38 | 122.91 (1.20) | 123.03 (1.10) | 122.78 (1.30) |
| 10 | 133.13 | 132.27 (0.65) | 132.48 (0.49) | 132.28 (0.64) |
| 11 | 168.91 | 168.55 (0.21) | 168.91 (0.00) | 169.01 (0.06) |
| 12 | 197.19 | 196.91 (0.14) | 196.74 (0.23) | 197.90 (0.36) |
| 13 | 203.91 | 204.45 (0.26) | 204.09 (0.09) | 204.95 (0.51) |
| 14 | 225.47 | 225.46 (0.00) | 225.73 (0.12) | 225.08 (0.18) |
| 15 | 229.69 | 229.72 (0.01) | 229.65 (0.02) | 228.39 (0.57) |

can be found as Supplementary Fig. S1(b) online. The population size, number of generations, generation gap, probability of crossover, and probability of mutation as GA parameters were set as 100, 100, 0.9, 0.6, and 0.05, respectively. The search capability of GA for the PUC analysis was also investigated by solving a benchmark problem, which indicated that it has a high search capability under the conditions used in this study (details can be found in the Supplementary Information).

## 3. Results and discussion

**Resonance frequency measurements.** First, the values and number of resonance frequencies to be used for comparison between the experiment and FE analysis were determined. The amplitude–frequency response of the nacre sample obtained from vibration testing is shown in Fig. 4. As the spectrum contains many resonance peaks that provide no information on the vibrational modes, the correct vibrational modes must be identified to determine $C_{ij}$ inversely. To address this, we conducted a preliminary FE analysis and compared the results with the experimental vibration patterns. Consequently, clear vibrational mode matching was observed at 15 resonance frequencies, as indicated by the arrows in Fig. 4. The series of vibration patterns determined experimentally and by the preliminary FE analysis are shown in Fig. 5. Based on these observations, the equivalent elastic constants of nacre were investigated using the experimentally observed resonance frequencies, $\bar{f}_i$, listed in Table 1. Due to the plate-like shape of the sample, the sensitivity of the few first resonant modes is anticipated to be low to some of the elastic constants. However, the evaluation process used in this study is expected to identify five elastic constants, on the basis of the matching of vibration patterns at each resonance frequency and the identified search range for elastic constants based on the results of previous studies [3,24–34]. Furthermore, the authors' expectation is supported by the fact that they were able to identify the elastic constants of a plate-shape test sample with known elastic constants, as described in the Supplementary Information.

**Equivalent elastic constants of nacre.** For determining the equivalent elastic constants of nacre, the five elastic constants were optimized such that the 15 resonance frequencies calculated by FE analysis were equivalent to those obtained from the experiment. Supplementary Fig. S8 shows the relationship between the number of generations and the best fitness in each generation. As mentioned above, since the sensitivity to in-plane shear motion is anticipated to be low due to the thinness of the sample, optimization was performed under three different initial conditions to obtain different elastic constants for the first generation. $F_{\mathrm{RUS}}$ decreased rapidly with increasing number of generations and then plateaued approximately at the 20th generation regardless of the differences in the initial conditions. The combination of elastic constants that gave the best fitness at the 100th generation was considered as the optimal set of values. Experimentally measured $\bar{f}_i$ and numerically calculated $f_i$ are listed in Table 1; no significant difference was observed between the three FE calculation results and the maximum percentage error for each FE calculation was less than 4%. Furthermore, the vibration patterns at each resonance frequency were confirmed as identical to those determined experimentally, suggesting that the GA optimization process was performed well. The five optimized elastic constants of nacre and those reported by others [3,24–30] are summarized in Table 2. Limited data have been reported thus far by conventional mechanical testing approaches owing to the difficulty in measuring the shear stiffness and out-of-plane Poisson's ratio. The out-of-plane ($E^{\mathrm{n}}_{xx}$) and in-plane ($E^{\mathrm{n}}_{yy}$, $E^{\mathrm{n}}_{zz}$) Young's moduli of nacre determined in this study are 72.3 ± 1.7 and 74.8 ± 2.0 GPa, respectively, which are slightly different between the out-of-plane and in-plane directions. These observations are consistent with the results obtained by conventional mechanical testing methods [24,30]. One of the major advantages of the RUS technique is that full elastic constants can be determined in a single measurement. The RUS results revealed for the first time that the out-of-plane ($\upsilon^{\mathrm{n}}_{xy}$) and in-plane Poisson's ratio ($\upsilon^{\mathrm{n}}_{yz}$) and the out-of-plane shear modulus ($G^{\mathrm{n}}_{xy}$) of nacre, which have rarely been reported [25,27], are 0.23 ± 0.01, 0.24 ± 0.04, and 21.3 ± 0.9 GPa, respectively.

**Elastic constants of tablets.** The transverse isotropic elastic constants of the individual constituent tablets were determined by PUC analysis combined with GA optimization to ensure that the elastic constants acquired from the PUC analysis were equivalent to those obtained by RUS. As described in the Methods section, the elastic constants and volume fraction of the interlayer material were assumed to be known constant values. Thus, the variables were five elastic constants ($E^{\mathrm{t}}_{xx}$, $E^{\mathrm{t}}_{yy}$, $\nu^{\mathrm{t}}_{xy}$, $\nu^{\mathrm{t}}_{yz}$, and $G^{\mathrm{t}}_{xy}$) of the tablets. The fitness, $F_{\mathrm{PUC}}$, calculated from equation (4) decreased with increasing the number of generations and then flattened before reaching the 100th generation (Supplementary Fig. S9 online). Comparing the equivalent

**Table 2**
List of transverse isotropic elastic constants of nacre and those reported in the literature. The units of $E^{\mathrm{n}}_{xx}$, $E^{\mathrm{n}}_{yy}$, and $G^{\mathrm{n}}_{xy}$ are GPa.

| $E^{\mathrm{n}}_{xx}$ | $E^{\mathrm{n}}_{yy}$ | $\nu^{\mathrm{n}}_{xy}$ | $\nu^{\mathrm{n}}_{yz}$ | $G^{\mathrm{n}}_{xy}$ | Shell species | Method | Reference |
|---|---|---|---|---|---|---|---|
| 72.3 ± 1.7 | 74.8 ± 2.0 | 0.23 ± 0.01 | 0.24 ± 0.04 | 21.3 ± 0.9 | *Pinctada martensii* | RUS + GA | This study |
| 73 ± 9 | 70 ± 11 | – | – | – | *Pinctada* | Three-point bending test | 24 |
| – | 77 ± 12 | – | – | – | *Pinctada maxima* | Three-point bending test | 3 |
| 54.4 ± 3.2 to 62.5 ± 11.2 | – | 0.2 ± 0.03 to 0.25 ± 0.03 | – | – | *Pinctada maxima* | Indentation test | 25 |
| – | 66 ± 2 | – | – | – | *Haliotis rufescens* | Three-point bending test | 3 |
| 79 ± 15 | – | – | – | – | *Haliotis rufescens* | Indentation test | 26 |
| – | 90 | | 0.3 | – | *Haliotis rufescens* | Tensile test | 27 |
| 53.2–80.1 | – | – | – | – | *Haliotis rufescens* | Indentation test | 28 |
| 70 | – | – | – | – | *Haliotis rufescens* | Indentation test | 29 |
| 97.63 ± 5.31 | 79.75 ± 1.35 | – | – | – | *Abalone* | Atomic force microscopy | 30 |

**Table 3**
List of quantified elastic constants of nacre tablets and those reported in the literature. The units of $E^{t}_{xx}$, $E^{t}_{yy}$, and $G^{t}_{xy}$ are GPa.

| $E^{t}_{xx}$ | $E^{t}_{yy}$ | $\nu^{t}_{xy}$ | $\nu^{t}_{yz}$ | $G^{t}_{xy}$ | Shell species | Method | Reference |
|---|---|---|---|---|---|---|---|
| 72.7 | 75.0 | 0.21 | 0.24 | 21.3 | *Pinctada martensii* | PUC + GA | This study |
| 96.75 ± 5.67 | – | 0.17 ± 0.05 | – | – | *Pinctada maxima* | Indentation test | 25 |
| 82.7 | – | – | – | – | *Haliotis rufescens* | Indentation test | 26 |
| 69 ± 7 | – | – | – | – | *Haliotis rufescens* | Indentation test | 34 |
| 103.1 | 87.00 | – | – | – | *Abalone* | Atomic force microscopy | 30 |

elastic constants of the nacre obtained by RUS and PUS analysis at the 100th generation, the maximum percentage error was small (Supplementary Table S7), indicating that the optimization was performed well. The optimized tablet elastic constants and those reported by others [25,26,30,34] are summarized in Table 3. In this study, we assumed the geometrical configuration of the polygonal tablets to have a cuboid shape, but the optimized variables fall within the range of experimentally determined values. The calculated out-of-plane ($E^{t}_{xx}$) and in-plane moduli ($E^{t}_{yy}$) were slightly larger than those of nacre ($E^{n}_{xx}$ and $E^{n}_{yy}$) owing to the presence of interlayer materials with lower isotropic Young's modulus and the low volume fraction of interlayer material in nacre.

The range of reported Young's moduli of the interlayer material is wide, ranging from 2.84 to 49 GPa [25,26,31–34]. As the method for evaluating the tablet elastic constants in this study depends on the Young's modulus (and Poisson's ratio) of the interlayer material, the effects of the interlayer Young's modulus on the tablet elastic constants was further investigated using the lowermost and uppermost values of 2.84 [26] and 49 GPa [34], respectively. With a Young's modulus of 2.84 GPa and Poisson's ratio of 0.3 the calculated $E^{t}_{xx}$ and $E^{t}_{yy}$ were 76.1 and 78.1 GPa, respectively, whereas for modulus of 49 GPa and Poisson's ratio of 0.3, the values were 57.0 and 59.6 GPa, respectively (details on the optimization procedures and a full list of the elastic constants are provided in the Supplementary Information). These observations indicate that $E^{t}_{xx}$ and $E^{t}_{yy}$ of the tablets are in line with the reported Young's modulus under the conditions of interlayer Young's modulus in the range of 2.84–49 GPa.

Creating tough, fracture-resistant materials that mimic the unique structural characteristics of biomaterials has been a central focus of materials science research. Numerical analyses have been conducted to understand the toughening and deformation mechanisms of nacre, but all were based on the assumption of isotropic characteristics for nacre and its constituent tablets or on unfounded elastic constants. This study is the first in which the transverse isotropic elastic constants were simultaneously determined by measuring the natural nacre vibrations. Furthermore, the transverse isotropic elastic constants of the constituent tablets were also determined based on the equivalent elastic constants of nacre obtained by RUS. These results may help to provide new insights into the toughening and deformation mechanisms of nacre and suggest a new design methodology for man-made nacreous composite materials with remarkable mechanical performance.

## 4. Conclusions

We have reported a combined experimental and numerical study in which we determined the transverse isotropic elastic constants of a nacre sample by utilizing the resonant vibration phenomenon observed in solid materials. The out-of-plane displacement distribution caused by resonant vibration of the nacre sample was measured using laser Doppler interferometry to unambiguously identify the vibration patterns. The measured Young's moduli in the out-of-plane and in-plane directions, 72.3 ± 1.7 and 74.8 ± 2.0 GPa, respectively, were characterized by near isotropy and are reasonably consistent with the literature data obtained by conventional experimental methods. Using the estimated equivalent elastic constants of nacre, we also determined the transverse isotropic elastic constants of the constituent tablets by implementing GA-assisted PUC analysis. The calculated out-of-plane and in-plane moduli of 72.7 and 75.0 GPa, respectively, were slightly higher than those of nacre, because of the presence of interlayer materials with the lower isotropic Young's modulus and the low volume fraction of organic interlayer polymer in nacre.

## Author statement

G.Y. designed the experiments. G.Y. performed experiments and collected data. G.Y., K.M. and S.Y. conducted the modeling. G.Y., K.M. and S.Y. analyzed the data. G.Y. and J.W.S. wrote the manuscript. G.Y. and J.W.S. edited the manuscript. All authors read and approved the final manuscript.

## Uncited references

[13].

## Declaration of competing interest

The authors declare that they have no known competing financial interests or personal relationships that could have appeared to influence the work reported in this paper.

## Acknowledgements

The authors thank Prof. T. Okabe and Dr. Y. Kumagai of the Department of Aerospace Engineering, Tohoku University for technical assistance in the FE and PUC analysis, Prof. M. Arai of the Department of Aerospace Engineering, Nagoya University for technical assistance in the GA analysis, and Mr. F. Bouteille of the Polytec Japan for technical assistance in the resonance spectrum and harmonic vibration pattern measurements. This work was partly supported by JSPS KAKENHI grant number 18K04721.

## Appendix A. Supplementary data

Supplementary data to this article can be found online at https://doi.org/10.1016/j.rinma.2022.100312.

## References

[1] B.L. Smith, et al., Molecular mechanistic origin of the toughness of natural adhesives, fibres and composites, Nature 399 (6738) (1999) 761–763, https://doi.org/10.1038/21607.
[2] S. Kamat, X. Su, R. Ballarini, A.H. Heuer, Structural basis for the fracture toughness of the shell of the conch Strombus gigas, Nature 405 (6790) (2000) 1036–1040, https://doi.org/10.1038/35016535.
[3] R.Z. Wang, Z. Suo, A.G. Evans, N. Yao, I.A. Aksay, Deformation mechanisms in nacre, J. Mater. Res. 16 (9) (2001) 2485–2493, https://doi.org/10.1557/JMR.2001.0340.
[4] A.G. Evans, et al., Model for the robust mechanical behavior of nacre, J. Mater. Res. 16 (9) (2001) 2475–2482, https://doi.org/10.1557/JMR.2001.0339.
[5] F. Song, A.K. Soh, Y.L. Bai, Structural and mechanical properties of the organic matrix layers of nacre, Biomaterials 24 (20) (2003) 3623–3631, https://doi.org/10.1016/S0142-9612(03)00215-1.
[6] K.S. Katti, D.R. Katti, S.M. Pradhan, A. Bhosle, Platelet interlocks are the key to toughness and strength in nacre, J. Mater. Res. 20 (5) (2005) 1097–1100, https://doi.org/10.1557/JMR.2005.0171.
[7] X. Li, Z.H. Xu, R. Wang, In situ observation of nanograin rotation and deformation in nacre, Nano Lett. 6 (10) (2006) 2301–2304, https://doi.org/10.1021/nl061775u.
[8] F. Barthelat, H. Tang, P.D. Zavattieri, C.M. Li, H.D. Espinosa, On the mechanics of mother-of-pearl: a key feature in the material hierarchical structure, J. Mech.

Phys. Solid. 55 (2) (2007) 306–337, https://doi.org/10.1016/j.jmps.2006.07.007.
[9] M.A. Meyers, A.Y.M. Lin, P.Y. Chen, J. Muyco, Mechanical strength of abalone nacre: role of the soft organic layer, J. Mech. Behav. Biomed. Mater. 1 (1) (2008) 76–85, https://doi.org/10.1016/j.jmbbm.2007.03.001.
[10] M.A. Meyers, et al., The role of organic intertile layer in abalone nacre, Mater. Sci. Eng. C 29 (8) (2009) 2398–2410, https://doi.org/10.1016/j.msec.2009.07.005.
[11] Z. Huang, X. Li, Origin of flaw-tolerance in nacre, Sci. Rep. 3 (2013) 1693, https://doi.org/10.1038/srep01693.
[12] H. Ji, X. Li, D. Chen, Cymbiola nobilis shell: toughening mechanisms in a crossed-lamellar structure, Sci. Rep. 7 (2017) 40043, https://doi.org/10.1038/srep40043.
[13] Z. Tang, N.A. Kotov, S. Magonov, B. Ozturk, Nanostructured artificial nacre, Nat. Mater. 2 (6) (2003) 413–418, https://doi.org/10.1038/nmat906.
[14] G. Yamamoto, et al., Mechanical properties of binder-free single-walled carbon nanotube solids, Scripta Mater. 54 (2) (2006) 299–303, https://doi.org/10.1016/j.scriptamat.2005.03.053.
[15] X. Hu, Z. Xu, C. Gao, Multifunctional, supramolecular, continuous artificial nacre fibres, Sci. Rep. 2 (2012) 767, https://doi.org/10.1038/srep00767.
[16] F. Bouville, et al., Strong, tough and stiff bioinspired ceramics from brittle constituents, Nat. Mater. 13 (5) (2014) 508–514, https://doi.org/10.1038/nmat3915.
[17] G. Yamamoto, et al., Fabrication and mechanical evaluation of aligned multi-walled carbon nanotube sheet/alumina laminated ceramic composites, in: 16th European Conference on Composite Materials, 2014 2014.
[18] H. Kessler, R. Ballarini, R.L. Mullen, L.T. Kuhn, A.H. Heuer, A biomimetic example of brittle toughening: (I) steady state multiple cracking, Comput. Mater. Sci. 5 (1–3) (1996) 157–166, https://doi.org/10.1016/0927-0256(95)00067-4.
[19] R. Menig, M.H. Meyers, M.A. Meyers, K.S. Vecchio, Quasi-static and dynamic mechanical response of Haliotis rufescens (abalone) shells, Acta Mater. 48 (9) (2000) 2383–2398, https://doi.org/10.1016/S1359-6454(99)00443-7.
[20] R. Menig, M.H. Meyers, M.A. Meyers, K.S. Vecchio, Quasi-static and dynamic mechanical response of Strombus gigas (conch) shells, Mater. Sci. Eng., A 297 (1–2) (2001) 203–211, https://doi.org/10.1016/S0921-5093(00)01228-4.
[21] H. Gao, B. Ji, I.L. Jäger, E. Arzt, P. Fratzl, Materials become insensitive to flaws at nanoscale: lessons from nature, Proc. Natl. Acad. Sci. U. S. A. 100 (10) (2003) 5597–5600, https://doi.org/10.1073/pnas.0631609100.
[22] S. Cui, Z. Lu, Z. Yang, Effect of interlocking structure on mechanical properties of bio-inspired nacreous composites, Compos. Struct. 226 (2019) 111260, https://doi.org/10.1016/j.compstruct.2019.111260.
[23] S. Cui, Z. Yang, Z. Lu, An analytical model for the bio-inspired nacreous composites with interlocked "brick-and-mortar" structures, Compos. Sci. Technol. 193 (2020) 108131, https://doi.org/10.1016/j.compscitech.2020.108131.
[24] A.P. Jackson, J.F.V. Vincent, R.M. Turner, The mechanical design of nacre, Proc. R. Soc. London, Ser. A or B 234 (1988) 415–440, https://doi.org/10.1098/rspb.1988.0056.
[25] P. Stempflé, O. Pantalé, M. Rousseau, E. Lopez, X. Bourrat, Mechanical properties of the elemental nanocomponents of nacre structure, Mater. Sci. Eng. C 30 (5) (2010) 715–721, https://doi.org/10.1016/j.msec.2010.03.003.
[26] F. Barthelat, C.M. Li, C. Comi, H.D. Espinosa, Mechanical properties of nacre constituents and their impact on mechanical performance, J. Mater. Res. 21 (8) (2006) 1977–1986, https://doi.org/10.1557/jmr.2006.0239.
[27] F. Barthelat, H.D. Espinosa, An experimental investigation of deformation and fracture of nacre-mother of pearl, Exp. Mech. 47 (3) (2007) 311–324, https://doi.org/10.1007/s11340-007-9040-1.
[28] X. Li, W.C. Chang, Y.J. Chao, R. Wang, M. Chang, Nanoscale structural and mechanical characterization of a natural nanocomposite material: the shell of red abalone, Nano Lett. 4 (4) (2004) 613–617, https://doi.org/10.1021/nl049962k.
[29] J. Bezares, Z. Peng, R.J. Asaro, Q. Zhu, Macromolecular structure and viscoelastic response of the organic framework of nacre in Haliotis rufescens: a perspective and overview, Theor. Appl. Mech. 38 (2) (2011) 75–106, https://doi.org/10.2298/TAM1102075B.
[30] T. Li, K. Zeng, Nanoscale elasticity mappings of micro-constituents of abalone shell by band excitation-contact resonance force microscopy, Nanoscale 6 (4) (2014) 2177–2185, https://doi.org/10.1039/c3nr05292c.
[31] D.R. Katti, K.S. Katti, Modeling microarchitecture and mechanical behavior of nacre using 3D finite element techniques. Part I. Elastic properties, J. Mater. Sci. 36 (6) (2001) 1411–1417, https://doi.org/10.1023/A:1017528209162.
[32] P. Stempflé, et al., Friction-induced sheet nacre fracture: effects of nano-shocks on cracks location, Int. J. Nanotechnol. 4 (6) (2007) 712–729, https://doi.org/10.1504/IJNT.2007.015466.
[33] H. Moshe-Drezner, D. Shilo, A. Dorogoy, E. Zolotoyabko, Nanometer-scale mapping of elastic modules in biogenic composites: the nacre of mollusk shells, Adv. Funct. Mater. 20 (16) (2010) 2723–2728, https://doi.org/10.1002/adfm.200902165.
[34] Z.H. Xu, Y. Yang, Z. Huang, X. Li, Elastic modulus of biopolymer matrix in nacre measured using coupled atomic force microscopy bending and inverse finite element techniques, Mater. Sci. Eng. C 31 (8) (2011) 1852–1856, https://doi.org/10.1016/j.msec.2011.08.023.
[35] B. Mohanty, K.S. Katti, D.R. Katti, Experimental investigation of nanomechanics of the mineral-protein interface in nacre, Mech. Res. Commun. 35 (1–2) (2008) 17–23, https://doi.org/10.1016/j.mechrescom.2007.09.006.
[36] Polytec GmbH, PSV-500 scanning vibrometer datasheet, Available from. http://www.polytec.com/us/products/vibration-sensors/scanning-vibrometers/psv-500-scanning-vibrometer/, 2016.
[37] J. Maynard, Resonant ultrasound spectroscopy, Phys. Today 49 (1) (1996) 26–31, https://doi.org/10.1063/1.881483.
[38] H. Ogi, K. Sato, T. Asada, M. Hirao, Complete mode identification for resonance ultrasound spectroscopy, J. Acoust. Soc. Am. 112 (6) (2002) 2553–2557, https://doi.org/10.1121/1.1512700.
[39] G. Yamamoto, S. Kurisaki, S. Atobe, T. Okabe, Determination of full elastic constants of carbon fiber in carbon fiber reinforced plastic composites, in: 33rd Technical Conference of the American Society for Composites 2018, 2018, pp. 1508–1514 No. 3.
[40] M. Tane, H. Okuda, F. Tanaka, Nanocomposite microstructures dominating anisotropic elastic modulus in carbon fibers, Acta Mater. 166 (2019) 75–84, https://doi.org/10.1016/j.actamat.2018.12.029.
[41] M. Arai, T. Suzuki, T. Yagi, K. Goto, Identification of anisotropic viscoelastic moduli of CFRP by measurement of resonant frequencies, Adv. Compos. Mater. 30 (1) (2021) 39–57, https://doi.org/10.1080/09243046.2020.1780370.
[42] D.E. Goldberg, Genetic algorithms in search, in: Optimization, and Machine Learning, Addison-Wesley Publishing Company, Boston, MA, 1989.
[43] J.H. Holland, Adaptation in Natural and Artificial Systems: an Introductory Analysis with Applications to Biology, Control, and Artificial Intelligence, MIT Press, Cambridge, MA, 1992.
[44] K. Deb, Multi-Objective Optimization Using Evolutionary Algorithms, John Wiley & Sons, Hoboken, NJ, 2001.
[45] M. Newman, A. Pipano, Fast modal extraction in NASTRAN via the FEER computer program, NASA TM X-2893 (1973) 485–506.
[46] B.N. Parlett, The Symmetric Eigenvalue Problem, Prentice-Hall, Englewood Cliffs, NJ, 1980.
[47] R.L. Haupt, S.E. Haupt, Practical Genetic Algorithms, John Wiley & Sons, Hoboken, NJ, 2004.
[48] ASTM International, Intel math kernel library documentation, Available from. https://software.intel.com/en-us/articles/intel-math-kernel-library-documentation/, 2012.